Simultaneous estimation of temperature and emissivity of metals around their melting points by deterministic and Bayesian techniques

Thomas Pierre, Jean-Claude Krapez, Helcio R.B. Orlande, Christophe Rodiet, Dylan Le Maux, Mickaël Courtois, Philippe Le Masson, Bernard Lamien

Simultaneous Estimation of Temperature and Emissivity of Metals around their Melting Points by Deterministic and Bayesian Techniques

Thomas Pierre[1], Jean-Claude Krapez[2], Helcio R. B. Orlande[3], Christophe Rodiet[4], Dylan Le Maux[1], Mickaël Courtois[1], Philippe Le Masson[1], Bernard Lamien[5]

[1] Univ. Bretagne Sud, FRE CNRS 3744, IRDL, F-56100 Lorient, France.

[2] ONERA - The French Aerospace Lab - Centre de Salon de Provence, France.

[3] Federal University of Rio de Janeiro, Rio de Janeiro, Brazil.

[4] Université de Reims Champagne Ardenne, ITheMM EA 7548, 51097 Reims, France.

[5] École Polytechnique de Ouagadougou (EPO), 18 BP 234, Ouagadougou, Burkina Faso.

Corresponding author: thomas.pierre@univ-ubs.fr

Abstract. This article presents the temperature and emissivity estimation of metals around their melting points using different techniques, which are based on deterministic (ordinary least squares) and Bayesian approaches. Linear and non-linear models are examined. The experimental data consist of radiative fluxes at six wavelengths, collected by a pyrometer. The apparatus is dedicated to the characterization of the physical properties of millimeter-sized metal samples at high temperatures, combining aerodynamic levitation and laser heating. Tests are performed on two metals: niobium with well-known temperature and steel.

1. Introduction

This article aims at the estimation of temperature and emissivity of metals above their melting points. It is a part of a global work dealing with the estimation of the physical properties of metals in solid and liquid states (density [1], viscosity, surface tension, diffusivity [2]). An apparatus, specifically developed, allows to perform aerodynamic levitation of samples of

millimeter size. Once in levitation, the samples are heated with a laser up to and above their melting temperature. Therefore, temperature measurements with thermocouple are not possible and non-contact measurements are necessary, such as pyrometry. Among all the instrumentations around the apparatus, a six-wavelength pyrometer collects the radiative flux in six narrow spectral bands.

The simultaneous estimation of temperature and emissivity of the sample is possible with bispectral or multispectral pyrometry. This technique is largely used in many fields, but presents several drawbacks. The major one is that the inversion problem is ill-posed in the sense that it is underdetermined; indeed in multiwavelength pyrometry there is always one unknown parameter more than there are equations [3]: for example in bispectral pyrometry, for two measurements at wavelengths λ_i and λ_j, there are three unknowns, the temperature and the two spectral emissivities ε_i and ε_j. Nevertheless, some possibilities exist to solve the problem; however they all require some assumptions.

The classical bispectral assumption is to consider a constant emissivity $\varepsilon_i \approx \varepsilon_j$ for two measurements at wavelengths λ_i and λ_j not to far from each other, and nevertheless not to close to not increase the temperature uncertainty [4]. In the case of the multiwavelength pyrometry, that is, for more than two wavelengths, it is common to use a mathematical or physical spectral model for the emissivity, on the condition that the number of unknowns is smaller than the number of wavelengths [5]. The model choice depends on the spectral range width of the pyrometer, and a low-order polynomial (order 1 or 2) form can be sufficient. However, a common result is that the identification error is highly sensitive to the matching of the chosen model with the real emissivity spectrum, which, by principle, is a difficult task since the real emissivity spectrum is not known beforehand [3], [6].

To solve the estimation problem three techniques are proposed here. The first one is based on bispectral pyrometry and ordinary least squares (OLS) coupled with a Levenberg-Marquardt

algorithm using two out of the six measurements with different possibilities of combinations [7]. The second technique is based on multispectral pyrometry and regularization by OLS estimation using a low-order model and some criteria allowing to not amplify the standard deviation on the estimated temperature [8].The third method is based on Bayesian inference, a stochastic technique, which allows to take into account *a priori* information about the parameters to be estimated [9]. The present work is developed as follows. First the apparatus and the six-wavelength pyrometer are presented in section 2. Section 3 is dedicated to theoretical considerations regarding the apparatus. The parameter estimation methodologies are presented in section 4, which are finally used in the last section 5 with the experimental data obtained from measurements with two metallic samples: niobium with known melting temperature (1 750 K) [13], and a steel sample, which has not been characterized, but according to ASTM, its melting temperature is about 1 697 K [14].

2. The levitation apparatus and the pyrometers

Figure 1 presents the apparatus dedicated to the levitation of spherical sample with a diameter of 3 mm. The levitation is assured by a controlled argon flow. Once in levitation the sample is heated above its melting point by a laser (300 W, 1.070 μm). Figure 1 shows also infrared and high-speed cameras that are not dealt in this study. The six-wavelength pyrometer is aimed at the sample top surface.

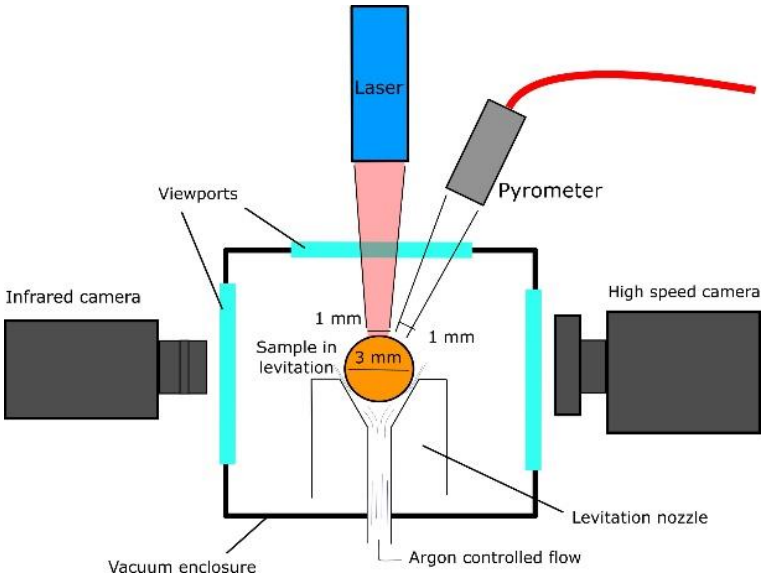

Figure 1. Sketch of the aerodynamic levitation apparatus

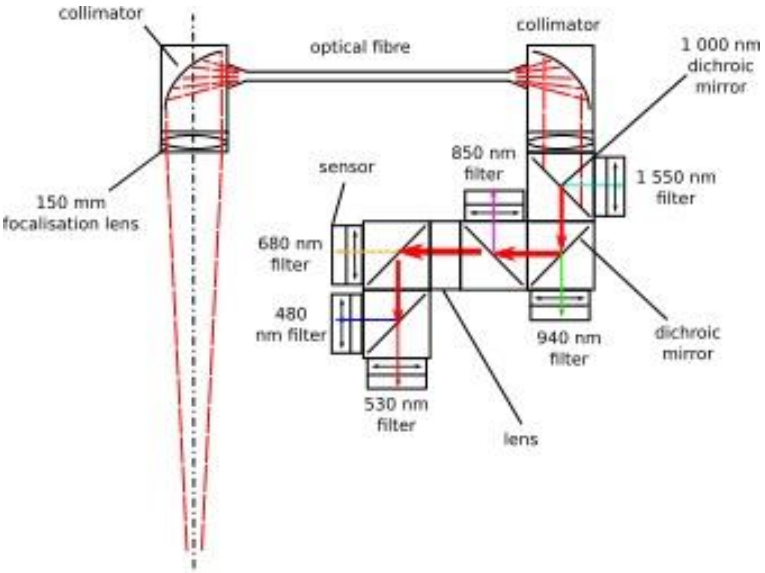

Figure 2. Sketch of the six-wavelength pyrometer.

The six-wavelength pyrometer is detailed in Figure 2. It is composed of collimators, lenses, dichroic mirrors, monochromatic filters, and silicon (Si) sensors. The six wavelengths that have been selected for applications above 1 000 K, are the following: 0.480 µm, 0.530 µm, 0.680 µm, 0.850 µm, 0.940 µm, and 1.550 µm. The diameter of the focused area is 2 mm and

the integration time is about 20 ms. The sensors can measure fluxes in the range [50 nW – 50 mW].

A commercial pyrometer, which does not appear in Figure 1, is also associated to the six-wavelength one. It is bispectral with wavelengths 0.900 µm and 1.050 µm. Therefore, as the laser wavelength is within its spectral band during the sample heating, the measurements of the pyrometer can only be used during the cooling of the sample, meaning when the laser is stopped. The parameter of the bispectral pyrometer to set is an emissivity ratio.

For both niobium and steel samples, the heating procedure is as follows: 140 W during 1 s, then 30 W for another five seconds.

3. Theoretical considerations

The flux $\Phi_i^{th}(T)$ collected by the i^{th} sensor is expressed theoretically by the following expression:

$$\Phi_i^{th}(T) = H_i \int_0^{\infty} f_i(\lambda)\varepsilon_i(\lambda,T)M^0(\lambda,T)d\lambda \qquad (1)$$

where T is the temperature (in kelvin), λ is the wavelength (in µm), H_i is an amplitude correction coefficient estimated by calibration, $f_i(\lambda)$ is the spectral transfer function of the i^{th} optical path (OP#i) gathering all the optical manufacturing data (*e.g.* spectral transmittivity), $\varepsilon_i(\lambda,T)$ is the sample surface emissivity, and $M^0(\lambda,T)$ is the Planck's law given by equation (2). This equation can be rewritten by using the Wien's approximation as equation (3) which is valid for λT less than 3 000 µm·K, which is mostly the case here [3]. In the case of a blackbody at temperature T, the theoretical flux collected is $\Phi_i^{0,th}(T)$.

$$M^0(\lambda, T) = \frac{C_1 \lambda^{-5}}{e^{\frac{C_2}{\lambda T}} - 1} \tag{2}$$

$$M^0(\lambda, T) = C_1 \lambda^{-5} e^{-\frac{C_2}{\lambda T}} \tag{3}$$

with $C_1 = 3.741 \times 10^8$ W·μm^4·m^{-2} and $C_2 = 14\,388$ μm·K [15]. It is assumed that the influence of both the environment and the atmosphere inside the apparatus are negligible.

Whatever the relation used to express the theoretical flux, (2) or (3), the signal is experimentally contaminated by an additive random noise e_i. Thus, let's define the observable Y_i as following:

$$Y_i = \varepsilon_i(T)\, \Phi_i^{0,th}(T) + e_i \tag{4}$$

Section 4.3 will present the temperature-emissivity estimation through the Bayesian technique using a linear approximation. Therefore, assuming Wien's approximation (3), and introducing mean values λ_i, ε_i and f_i for the wavelength, the emissivity and the transfer function, respectively, in each spectral band *i*. The flux in the band *i* can thus be simplified to:

$$\Phi_i^{th}(T) = H_i f_i \varepsilon_i C_1 \lambda_i^{-5} e^{-\frac{C_2}{\lambda_i T}} \tag{5}$$

The mean wavelengths λ_i are gathered in Table 1. The relation (5) can be linearized by taking the logarithm, by which the observable Y' is now:

$$Y_i' \equiv ln\left(\frac{\Phi_i^{th}(T)\lambda_i^5}{C_1 H_i f_i}\right) = ln(\varepsilon_i) - \mu_i \frac{T_{ref}}{T} + e_i' \tag{6}$$

The new observables are now $\mathbf{Y}' = [Y_1', Y_2', \ldots Y_m']^{\boldsymbol{T}}$ and in relation (6) μ_i is defined by (7), T_{ref} is an arbitrary reference temperature used for scaling the temperature, and e_i' is a Gaussian additive experimental error affecting the observables Y_i'. e_i' differs from e_i because of the linearization.

$$\mu_i = \frac{C_2}{\lambda_i T_{ref}} \tag{7}$$

The parameters of interest to estimate are the temperature and the emissivity. And one of the error sources comes from the spectral transfer functions $f_i(\lambda)$, that is why the H_i coefficients have been introduced and estimated by calibration against a blackbody. As an example Figure 3 presents the evolution of both the commercial bispectral pyrometer temperature and the OP#5 flux versus time during the cooling of a blackbody, that is, after the laser heating is stopped. Note that this blackbody has been placed in the levitation apparatus instead of the levitation nozzle (Figure 1). The estimation of H_i has been performed by solving equation (8), considering the temperature given by the commercial bispectral pyrometer as being the real one and the emissivity of the blackbody simulator being equal to one.

$$\Phi_i^{0,th}(H_i) = Y_i \tag{8}$$

The evolution of H_5 is plotted in Figure 4. Except during the very first period of time when the blackbody temperature is not uniform, the estimation of H_5 gives rather constant values; Figure 5 presents the histogram of the constant H_5 from which, assuming a Gaussian

distribution, the mean and the standard deviation are calculated. Table 1 gathers all results for the six optical paths.

Table 1. Means values and standard deviations of the H_i coefficients.

OP#i	**1**	**2**	**3**	**4**	**5**	**6**
$\boldsymbol{\lambda_i}$ **(µm)**	0.483	0.532	0.680	0.851	0.940	1.554
$\boldsymbol{\bar{H}_i \times 10^9}$	32.68	2.23	3.82	2.46	3.22	3.63
$\boldsymbol{\sigma_{H_i} \times 10^{11}}$	91.31	2.64	2.19	1.10	1.25	2.86

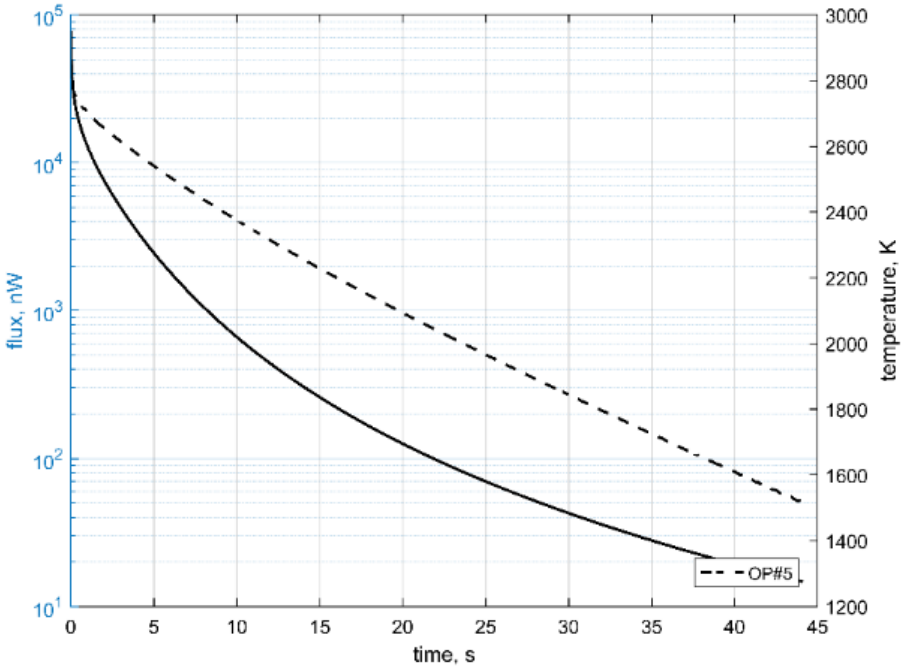

Figure 3. Evolution of the commercial bispectral pyrometer temperature (solid line) and of the OP#5 flux (dashed line) versus time during the calibration by means of a blackbody.

The mean values of the amplitude correction coefficients and the associated standard deviations are information of prime importance. Firstly, they allow to discuss the credibility of the estimated parameters. Secondly, they will be used for the Bayesian inference as *a priori*

information [9], so that their uncertainties are taken into account as regards the estimation of the parameters of interest, that is, the temperature and the emissivity of the sample (see section 4.3).

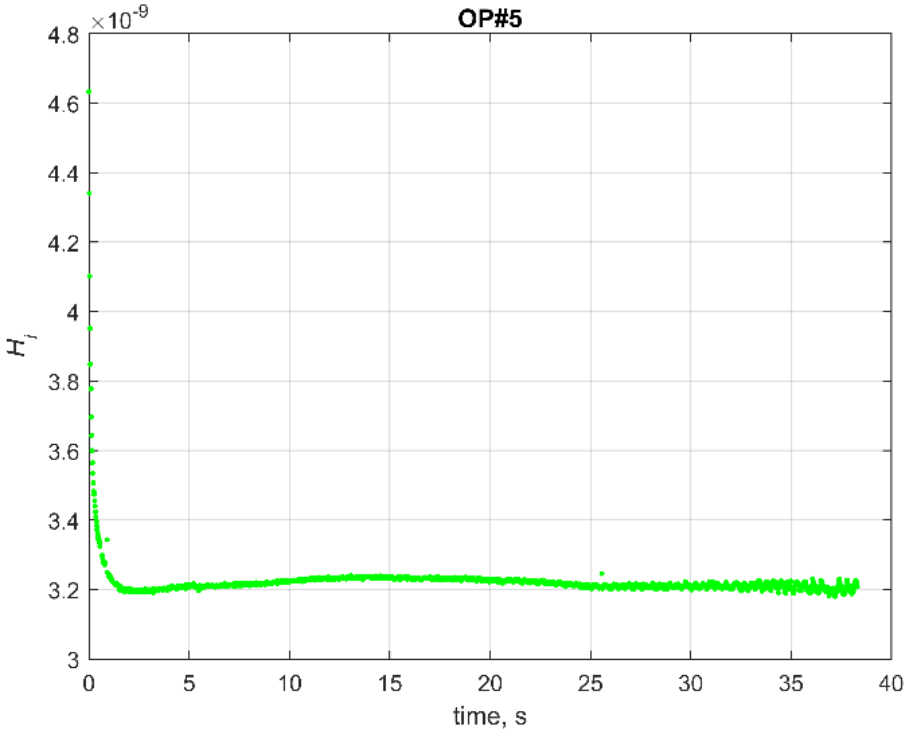

Figure 4. Example of estimating the H_5 coefficient during calibration.

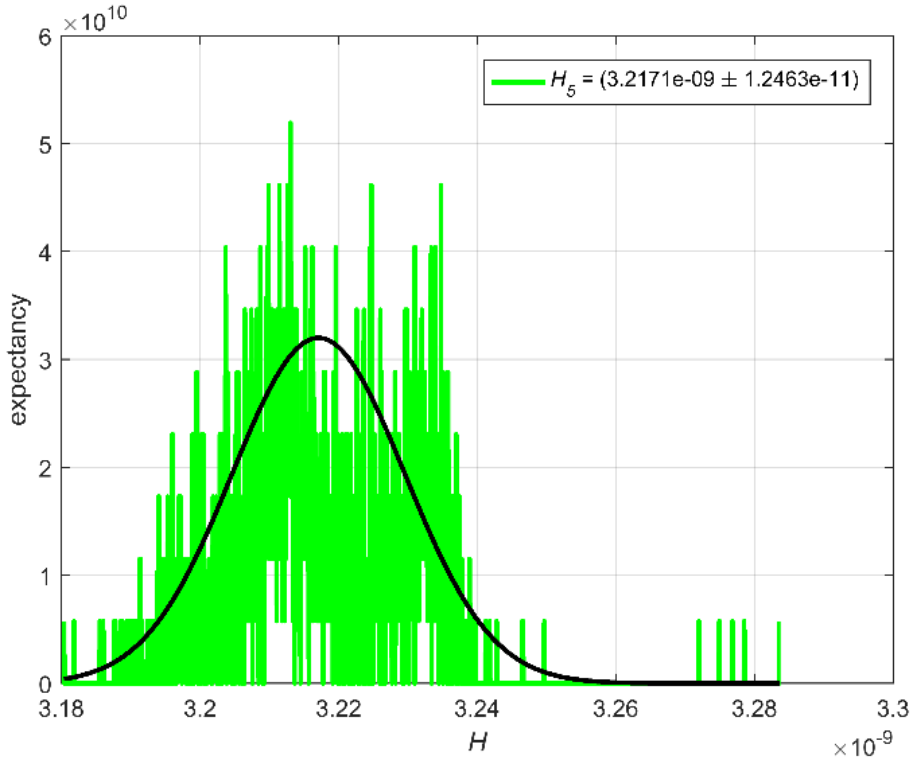

Figure 5. Gaussian representation of H_5.

4. Simultaneous estimation of Temperature and Emissivity

4.1. The bispectral method

Fundamentally, the bispectral method consists in estimating the temperature by using two radiative fluxes measured at wavelengths λ_i and λ_j. Regarding the spectral emissivity values, one of them is estimated in the same time as temperature, say ε_i at λ_i, whereas a functional relationship is assumed between ε_j (at λ_j) and ε_i. One possible functional relationship is $\varepsilon_j / \varepsilon_i = \xi_{ji}$ where ξ_{ji} is a predetermined constant. In the classical "greybody" approximation the constant ξ_{ji} is set to one, which, to be satisfactory, requires that the wavelengths λ_i and λ_j be not too far from each other.

Consider two radiative fluxes $\Phi_i^{exp}(T) \equiv Y_i$ and $\Phi_j^{exp}(T) \equiv Y_j$ measured at wavelengths λ_i and λ_j. The method lays on the simultaneous temperature emissivity estimation by solving the system (9)-(10):

$$\Phi_i^{th}(\varepsilon_i, T_{ij}) = Y_i \tag{9}$$

$$\xi_{ji}\Phi_j^{th}(\varepsilon_i, T_{ij}) = Y_j \tag{10}$$

where the coefficient ξ_{ji} is the assumed emissivity ratio $\varepsilon_j/\varepsilon_i$, which is 1 in the classical "greybody" approximation.

4.2. The multispectral method

In the case of multispectral pyrometry, that is to say using three and more wavelengths, the emissivity can be considered in terms of a low order polynomial form (11) even if some physical models exist (*e.g.* Drude, Hagen-Rubens [5]).

$$\varepsilon(\lambda, T) = \sum_{k=0}^{m} a_k \lambda^k \tag{11}$$

The proposed method here implies to correct the experimental flux Y_i by $Y_i^{cor} = Y_i/H_i f_i$ according to the linearization of the Planck's law (1). In order to not amplify the standard deviation on the estimated temperature and emissivity by multispectral methods, a parsimonious model is preferable, that is, the parametrization of a spectral emissivity of order 2 maximum, m = 0, 1, or 2 in (11), and a minimum distance between two consecutive wavelengths [4][8][16][17] expressed by relation (12). The objective is to minimize the cost function (13), where W is the number of considered wavelengths, $\Phi_i^{th,cor}$ is the corrected

theoretical flux using the Planck's law (without $H_i f_i(\lambda)$), and $\mathbf{a} = [a_0, \dots a_W]^T$ is the parameter vector of the emissivity model (11).

$$\Delta\lambda_{ij,min} = \left.\frac{\lambda_i^2 T}{C_2}\right|_{\lambda_i > \lambda_j} \tag{12}$$

$$\sum_{i=1}^{W} \left[\Phi_i^{th,cor}(T, \mathbf{a}) - Y_i^{corr}\right]^2 \tag{13}$$

4.3. Estimation by Bayesian inference

The Bayesian theorem is given in reference [12]:

$$\pi(\boldsymbol{\beta}|\mathbf{Y}) = \frac{\pi(\mathbf{Y}|\boldsymbol{\beta})\pi(\boldsymbol{\beta})}{\pi(\mathbf{Y})} \tag{14}$$

$$\boldsymbol{\beta} = [\boldsymbol{\varepsilon}, T]^T \tag{15}$$

where $\boldsymbol{\beta}$ is the vector of the following parameters: the temperature and the emissivities $\boldsymbol{\varepsilon} = [\varepsilon_1, \dots \varepsilon_m]^T$, where m represents the number of wavelengths. $\pi(\mathbf{Y}|\boldsymbol{\beta})$ is the likelihood function or the probability density of the measurements with the parameters $\boldsymbol{\beta}$ given, $\pi(\boldsymbol{\beta})$ is the *a priori* density of the unknown or uncertain parameters, and $\pi(\mathbf{Y})$ is the marginal probability density of the measurements, which plays the role of a normalization constant. As per equation (6), measurement uncertainties are supposed Gaussian with known zero mean and a covariance matrix, additive and independent from the unknown parameters. Thus, the likelihood function can be written:

$$\pi(\mathbf{Y}|\boldsymbol{\beta}) \propto exp\left\{-\frac{1}{2}\left[\mathbf{Y}-\boldsymbol{\varepsilon}\otimes\boldsymbol{\Phi}^{\mathbf{0},\boldsymbol{th}}(T)\right]^{T}\boldsymbol{\Omega}^{-1}\left[\mathbf{Y}-\boldsymbol{\varepsilon}\otimes\boldsymbol{\Phi}^{\mathbf{0},\boldsymbol{th}}(T)\right]\right\} \quad (16)$$

where $\boldsymbol{\Omega}$ is the measurement error covariance matrix and $\otimes$ denotes the element-wise product. Regarding the density of an *a priori* distribution of the parameters, it was assumed independent and given by (17), where $\pi(\boldsymbol{\varepsilon})$ and $\pi(\mathrm{T})$ are the probability densities of the emissivity and the temperature, respectively:

$$\pi(\boldsymbol{\beta}) = \pi(\boldsymbol{\varepsilon})\pi(T) \quad (17)$$

4.3.1. Multiwavelength pyrometer in linear approximation

In the case of the linear approximation, let's consider the system (5)-(7). Equation (6) can be rewritten as:

$$\mathbf{Y} = \mathbf{X}\boldsymbol{\beta} + \mathbf{e}' \quad (18)$$

$$\mathbf{X} = [\mathbf{I_{mm}} \quad -\boldsymbol{\mu}_{\boldsymbol{m1}}] \quad (19)$$

$$\boldsymbol{\mu} = [\mu_1\ \mu_2\ \ldots\ \mu_m]^T \quad (20)$$

where $\mathbf{I_{mm}}$ is the identity matrix of size m × m. Thus the relation (16) becomes, taking into account equation (17) and the linear hypothesis:

$$\pi(\boldsymbol{\beta}|\mathbf{Y}) \propto exp\left\{-\frac{1}{2}[(\mathbf{Y}-\mathbf{X}\boldsymbol{\beta})^{T}\boldsymbol{\Omega}^{-1}(\mathbf{Y}-\mathbf{X}\boldsymbol{\beta}) + (\boldsymbol{\beta}-\boldsymbol{\beta}^{\boldsymbol{prior}})^{T}\mathbf{W}^{-1}(\boldsymbol{\beta}-\boldsymbol{\beta}^{\boldsymbol{prior}})]\right\} \quad (21)$$

The maximum a posteriori (MAP) estimator is then obtained when its derivative is null with respect to the parameter vector. Introducing the MAP estimator and the posterior covariance matrix, relation (21) becomes:

$$\pi(\boldsymbol{\beta}|\mathbf{Y}) \propto \left\{-\frac{1}{2}\left[\left(\boldsymbol{\beta}-\widehat{\boldsymbol{\beta}}_{MAP}\right)^{T}\boldsymbol{\Gamma}_{\boldsymbol{\beta}|\mathbf{Y}}{}^{-1}\left(\boldsymbol{\beta}-\widehat{\boldsymbol{\beta}}_{MAP}\right)\right]\right\} \tag{22}$$

In relation (22), $\hat{\beta}_{MAP}$ is the MAP estimator (23) and $\boldsymbol{\Gamma}_{\boldsymbol{\beta}|\mathbf{Y}}$ is the posterior covariance matrix (24). They are given by [15]:

$$\widehat{\boldsymbol{\beta}}_{MAP} = \boldsymbol{\beta}^{\mathbf{prior}} + \mathbf{W}\mathbf{X}^{\mathbf{T}}(\mathbf{X}\mathbf{W}\mathbf{X}^{\mathbf{T}} + \boldsymbol{\Omega})^{-1}(\mathbf{Y} - \mathbf{X}\boldsymbol{\beta}^{\mathbf{prior}}) \tag{23}$$

$$\boldsymbol{\Gamma}_{\boldsymbol{\beta}|\mathbf{Y}} = \mathbf{W} - \mathbf{W}\mathbf{X}^{\mathbf{T}}(\mathbf{X}\mathbf{W}\mathbf{X}^{\mathbf{T}} + \boldsymbol{\Omega})^{-1}\mathbf{X}\mathbf{W} \tag{24}$$

4.3.2. Multiwavelength pyrometry in non-linear estimation

In the non-linear case, the theoretical fluxes are calculated from relations (1), (2), and (4), that is, with Planck's law. The $\boldsymbol{\beta}$ vector of the parameter is the same as in eq. (17).

A sampling method based on the Markov Chain Monte Carlo (MCMC) method is used in this work. The Metropolis-Hastings algorithm was applied to generate samples of the posterior distribution based on the likelihood given by equation (16). This algorithm begins with the selection of a proposal distribution $p(\boldsymbol{\beta}^{*}, \boldsymbol{\beta}^{t-1})$, which is used to define a new candidate $\boldsymbol{\beta}$*, given the current state $\boldsymbol{\beta}^{t-1}$ of the Markov Chain. Once the proposal distribution is defined, the Metropolis-Hastings sampling algorithm can be implemented by repeating the following steps:

1- Sample a candidate $\boldsymbol{\beta}$* from the proposal distribution $p(\boldsymbol{\beta}^{*}, \boldsymbol{\beta}^{t-1})$.

2- Calculate the acceptance:

$$\alpha = min\left[1, \frac{\pi(\boldsymbol{\beta}^*|\mathbf{Y}), p(\boldsymbol{\beta}^*, \boldsymbol{\beta}^{\mathbf{t-1}})}{\pi(\boldsymbol{\beta}^{t-1}|\mathbf{Y}), p(\boldsymbol{\beta}^{t-1}, \boldsymbol{\beta})}\right] \quad (25)$$

3- Generate a random value U uniformly distributed between 0 and 1.

4- If $U \leq \alpha$, set $\boldsymbol{\beta}^t = \boldsymbol{\beta}^*$; otherwise, set $\boldsymbol{\beta}^t = \boldsymbol{\beta}^{t-1}$.

5- Return to step 1 to generate the sequence $\{\boldsymbol{\beta}^1, \boldsymbol{\beta}^2 \ldots, \boldsymbol{\beta}^n\}$.

In this manner, a sequence is generated to represent the *posterior* distribution, and inference on this posterior distribution is obtained from inference on the samples $\{\beta^1, \beta^2 \ldots, \beta^n\}$. Note that the values β^i must be rejected as long as the chain has not converged.

5. Results and discussions

5.1. Estimation with niobium

Figure 6 presents all the fluxes and temperature measurements during the experiment. The six continuous lines are the fluxes, the one at the bottom represents the flux at 0.48 µm wavelength while the one at the top corresponds to the 1.55 µm wavelength. The dashed line represents the temperature measured by the commercial bispectral pyrometer. As already mentioned above, this pyrometer works only during the cooling period due to wavelengths overlapping with the laser during heating. The melting and solidification plateaus are approximately at t = 1.2 s and 6.4 s, respectively.

The six-wavelength pyrometer offers numerous possible combinations to use the multispectral method for the parameter estimation. The bispectral method, presented in section 4.1, is now used, and two combinations are tested, the combination 3/4 due to literature data given at the wavelength of 0.680 µm, and the combination 4/5.

The two state changes (fusion, solidification), the large temperature variation, and the broad spectral range are three reasons that make the emissivity change highly likely. However, the niobium melting temperature is known (2 750 K) and the literature mentions values of emissivity around 0.35 at 0.684 5 µm in the liquid phase [13] and 0.35 at 0.650 µm in the solid phase [19], respectively. All these values are convenient to verify the estimations at the solidification plateau mainly, and useful as *a priori* data.

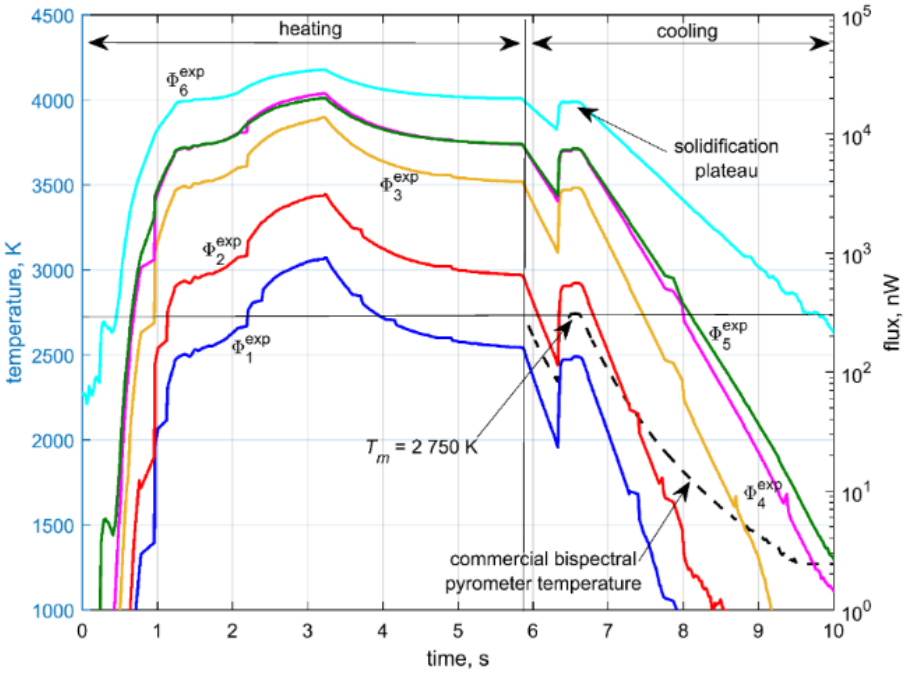

Figure 6. Niobium sample fluxes and commercial bispectral pyrometer temperature as a function of time.

We first analyze the solution of the system (9)-(10) by considering $\varepsilon_i = \varepsilon_j$, for two bispectral combinations and different initial guesses for temperature and emissivity, by comparison with literature values of the emissivity at the melting temperature. As the results are not satisfying, the greybody assumption should be relieved, which means that one should solve the system (9)-(10) by introducing an emissivity ratio ξ_{ji}. The estimation of this parameter is only possible using a known data, such as the solidification plateau.

This estimation is based on the experimental data, obtained during the cooling period, when the bispectral commercial pyrometer measures temperature T_{bis}. This minimization is based on a high confidence in the temperature given by the commercial bispectral pyrometer T_{bis}. Indeed, the measured temperature during the solidification plateau has been estimated at (2 731 ± 12) K (*i.e.* 0.5 %), which made it coincides with the literature [20], and its emissivity ratio has been set to 1.025 (consistent with ξ_{43}= 1.087, see further).

Results of two bispectral combinations are presented: 3/4 where $\Delta\lambda_{34}$ = 170 nm; 4/5 where $\Delta\lambda_{45}$ = 90 nm. Then the principle is to minimize the mean of the residuals (26) between the estimated temperature T_{ij} and T_{bis} during a short time interval (N = 50 between 5.9 s and 6.9 s).

$$\frac{1}{N}\sum_{k=1}^{N}\left[T_{ij}(t_k) - T_{bis}(t_k)\right]^2 \tag{26}$$

Figure 7 plots the evolution of the mean of residuals in eq. (23) versus ξ_{43}. Consequently, ξ_{43} = 1.087 and the results of emissivity and temperature, obtained for this value are presented in Figures 8 and 9. Even if the emissivity ratio has been evaluated during the short time interval of solidification, the obtained value has been applied to the whole duration of the experiment. Even if literature mentions a rather constant emissivity in the liquid state [13], this is a major assumption. Nevertheless, we can observe that in Figures 9 and 10 the estimated temperatures T_{34} and T_{45} are very close.

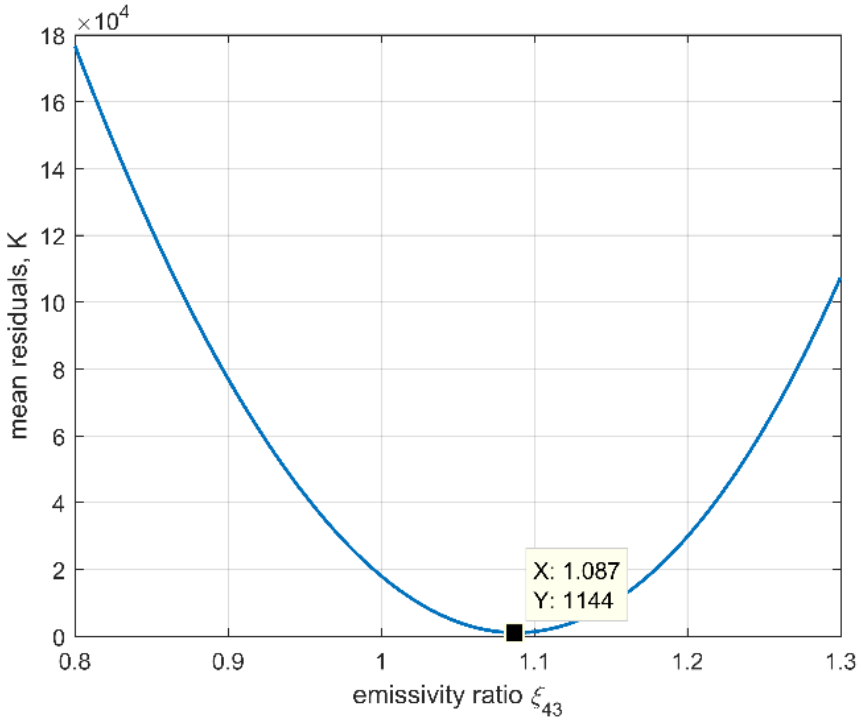

Figure 7. Residuals mean between the estimated temperature T_{34} and T_{bis} versus the emissivity ratio ξ_{43} during the cooling.

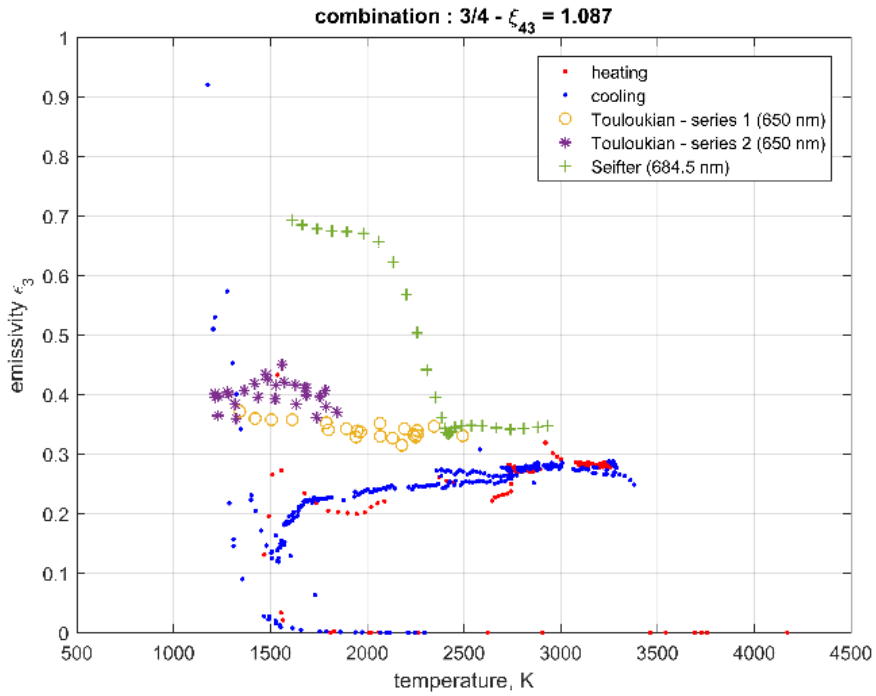

Figure 8. Estimated emissivity ε_3 (λ_3 = 0.68 µm) versus temperature and comparison with literature data at approximatively the same wavelength.

Figure 8 plots the evolution of the estimated emissivity ε_3 versus the estimated temperature T_{34}. Results are compared with niobium emissivity values, found in the literature. In the solid state, emissivity tends to decrease from 0.6 around 1 200 K to 0.3 until the liquefaction plateau, and are closer to Touloukian's than Seifter's value. However in the solid state, these emissivity and temperature are estimated values from fluxes recorded after 9 s (Figure 9), so they must be considered very carefully, since the fluxes are lower than 50 nW, which is at the lower limit of confidence of the sensor. Then in the liquid state, the emissivity is constant and just below 0.3 whereas the other values are rather between 0.3 and 0.4.

There is obviously a strong dispersion between measurements and literature values, and they are in the range 0.20 – 0.40. In our measurements, the samples are protected by an argon jet, limiting the oxidation. Nevertheless the major uncertainty concerns the blackbody calibration, as already mentioned in section 2. Although our estimated emissivities are more or less satisfying, new measurements are necessary to improve the confidence in our calibration. Indeed, an over- or underestimation on the H_i coefficient in relation (1) will directly lead to an under- or overestimation of the emissivity, respectively.

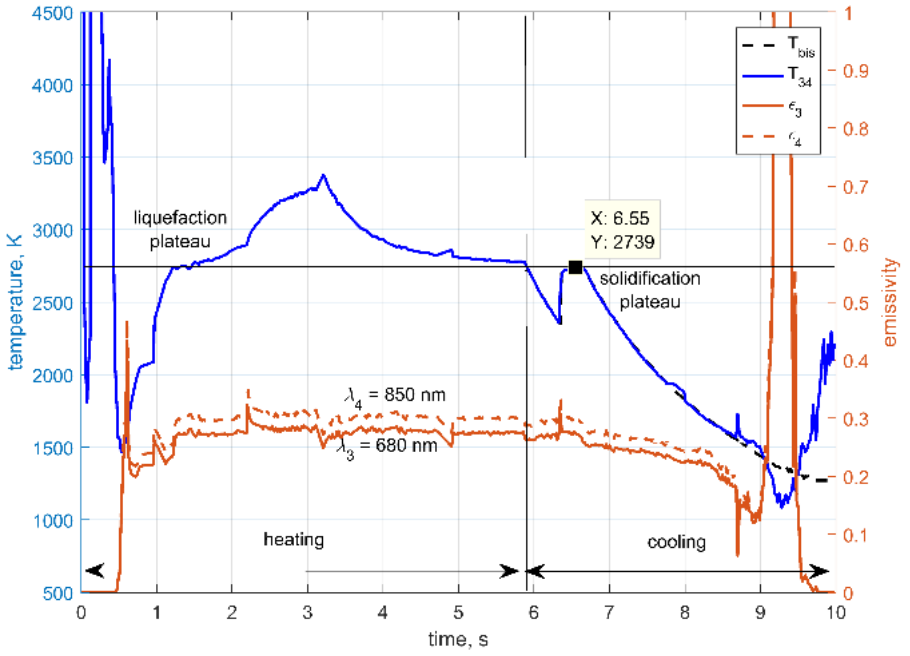

Figure 9. Bispectral temperature emissivity estimation for the combination 3/4.

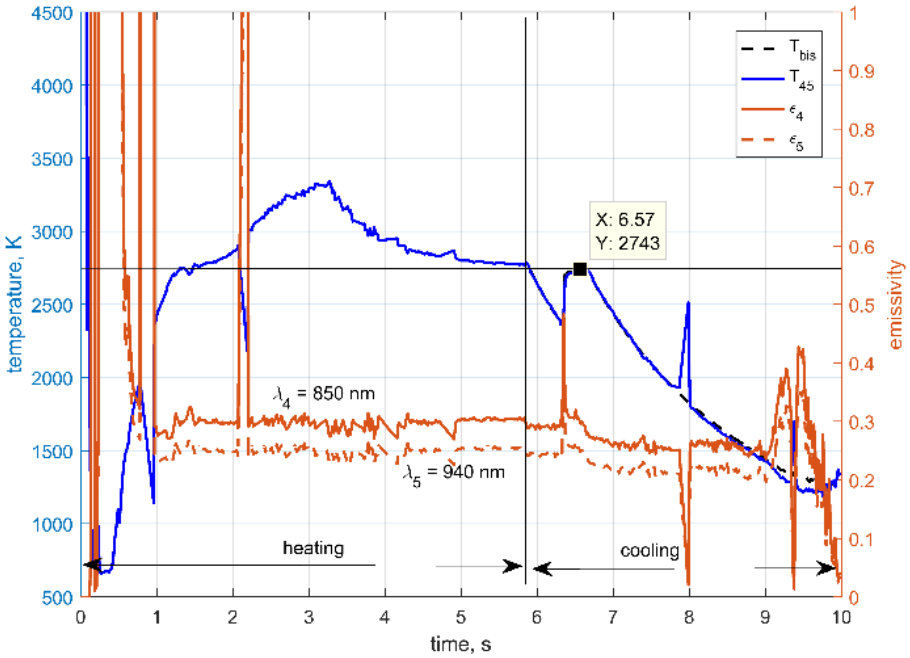

Figure 10. Bispectral temperature emissivity estimation for the combination 4/5.

Measurements on known materials, such as pure niobium, are convenient, since there is a possibility to have an *a priori* value such as the melting temperature as the point of reference.

But in the case of unknown materials, such as alloys, the solidification plateau would not be that constant but rather shows a slight decrease. This will be discussed in section 5.2. on the basis of the steel sample.

In the multispectral case (section 4.2), tests are performed considering emissivity as a polynomial of orders 0 (m = 0) and 1 (m = 1); the order 2 is not conceivable due to the spectral range being too narrow in the case of this study. Considering the six wavelengths, only four are kept to respect the minimal spectral criteria given by relation (12) with T = 2 750 K: λ_2 = 0.530 µm, λ_3 = 0.680 µm, λ_5 = 0.940 µm, and λ_6 = 1.055 µm. The estimation has been performed by ordinary least squares coupled with the Levenberg-Marquardt algorithm; estimated temperatures are presented in Figures 11 and 12. Figure 12 shows a difference of estimation between the two tested emissivity models. Nevertheless, estimated temperatures with the order 1 polynomial are better, since the temperature at the solidification plateau is estimated at (2 753 ± 20) K (0.8 %) (Figure 12). The order 0 polynomial overestimates the temperatures. This result is predictable, since the emissivity is considered constant along the spectral range [0.530 µm – 1.055 µm], which seems improbable with such a spectral range.

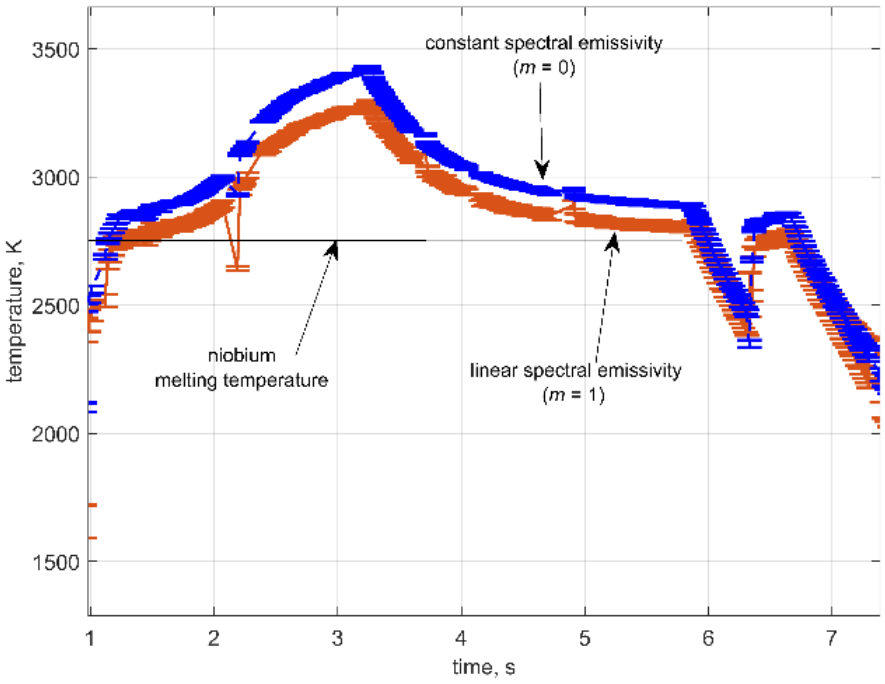

Figure 11. Estimated temperatures by multispectral method.

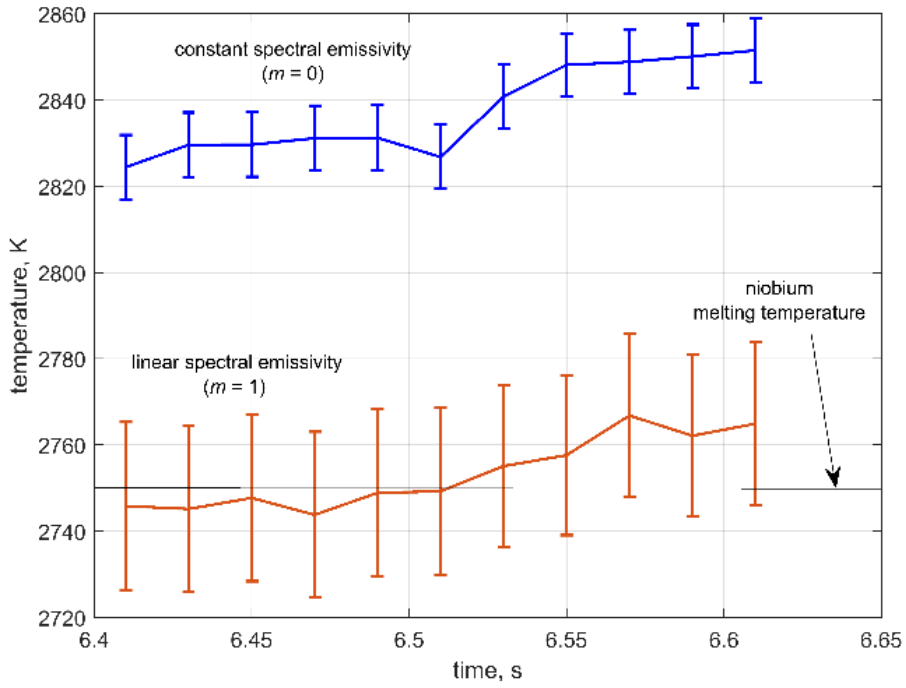

Figure 12. Zoom of the estimated temperatures at the solidification plateau.

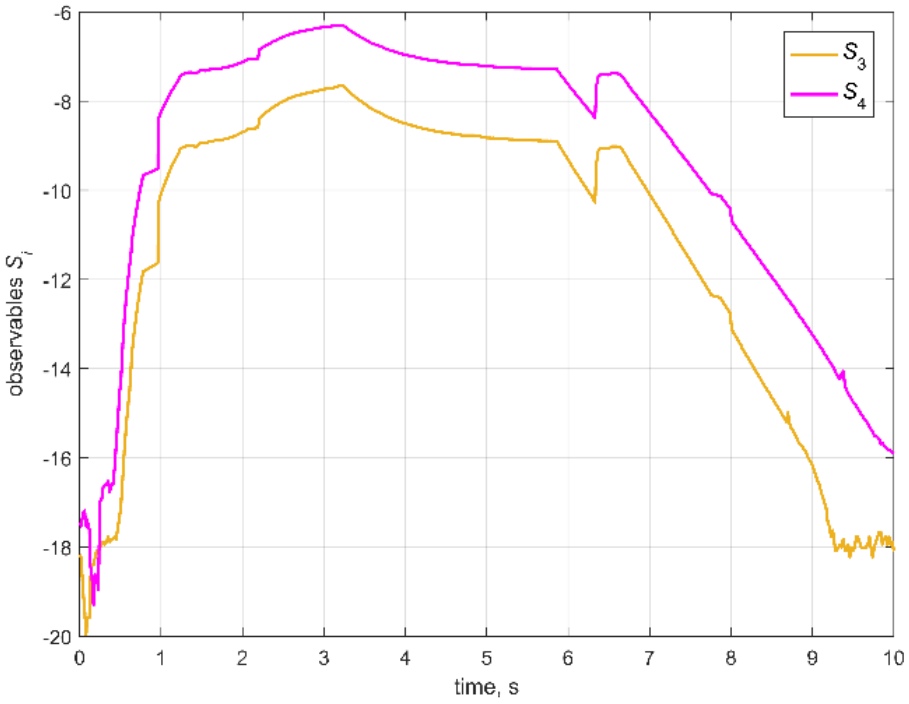

Figure 13. Modified observables for the combination 3/4 with Bayesian inference, considering linear approximation.

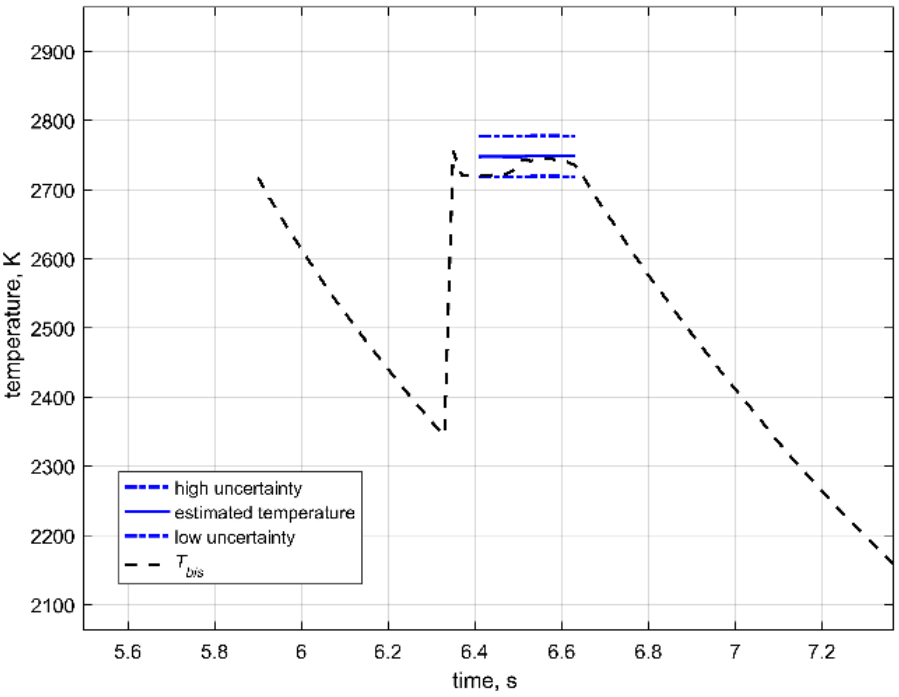

Figure 14. Estimated temperature around the melting point and comparison with T_{bis}.

Now parameter estimation is performed according to the Bayesian method in two ways: by a linear approximation (section 4.3.1) and in non-linear case, using MCMC (section 4.3.2). Only bispectral estimations are presented. To start with the linear approximation, the theoretical fluxes are linearized, as presented in relations (3),(5)-(7): Figure 13 presents them for the measurements of OP#3 and OP#4. Estimations are performed during the first part of the cooling, mainly during the solidification plateau.

Three parameters are considered: the temperature and the two emissivities. Tests are performed with different levels of confidence, with priors of good or bad quality. In the first stage we concentrated on the solidification plateau (Figure 14). Since the phase-change temperature is well known, we introduced a temperature prior of small uncertainty, T^{prior} = (2 750 ± 30) K whereas the emissivity priors were given a high uncertainty, namely ε_3^{prior} = ε_4^{prior} = 0.30 ± 0.15.

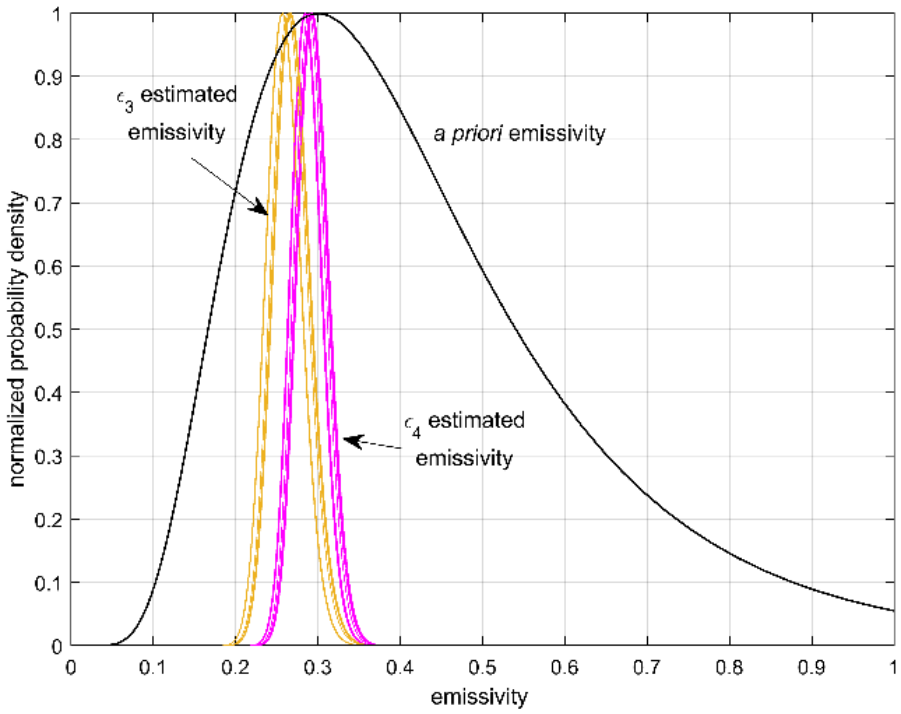

Figure 15. *A priori* and estimated emissivities ε_4 and ε_5 at the solidification plateau.

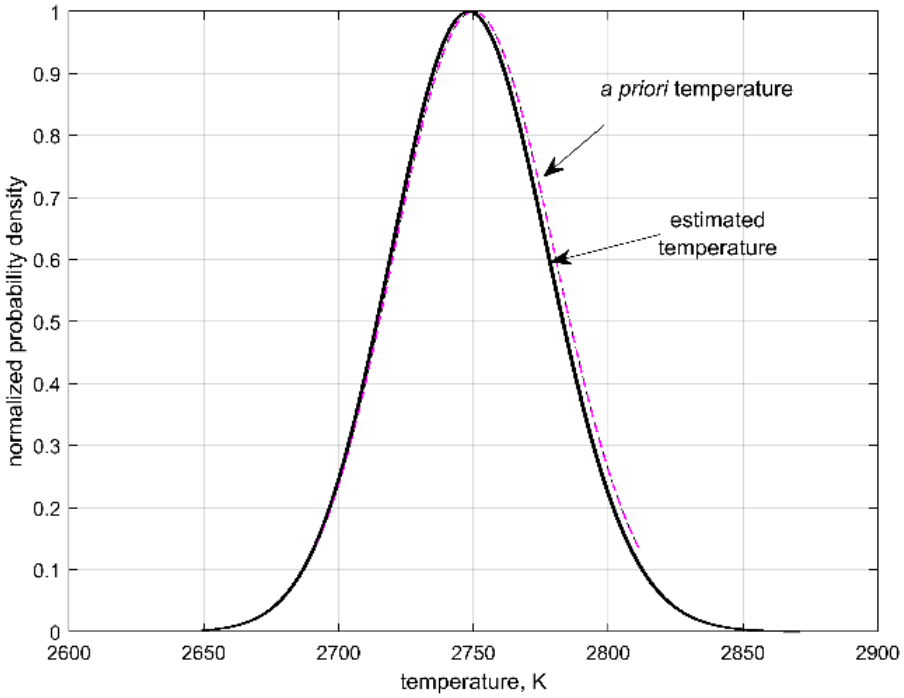

Figure 16. *A priori* and estimated temperature at the solidification plateau.

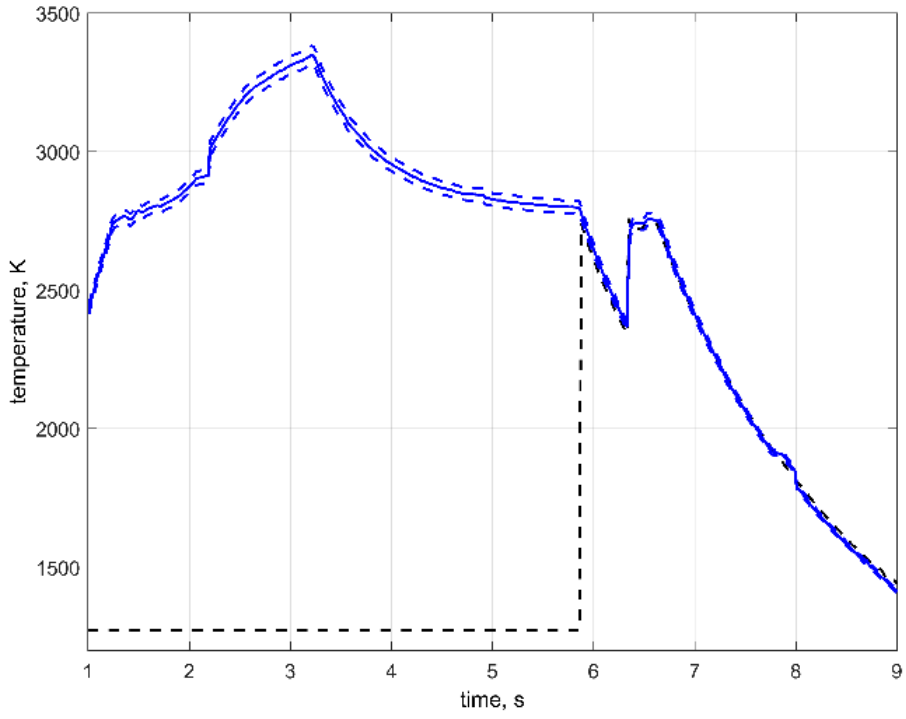

Figure 17. MAP estimator of temperature (in blue) with plus or minus one standard-deviation (dashed blue) and bispectral pyrometer (dashed black).

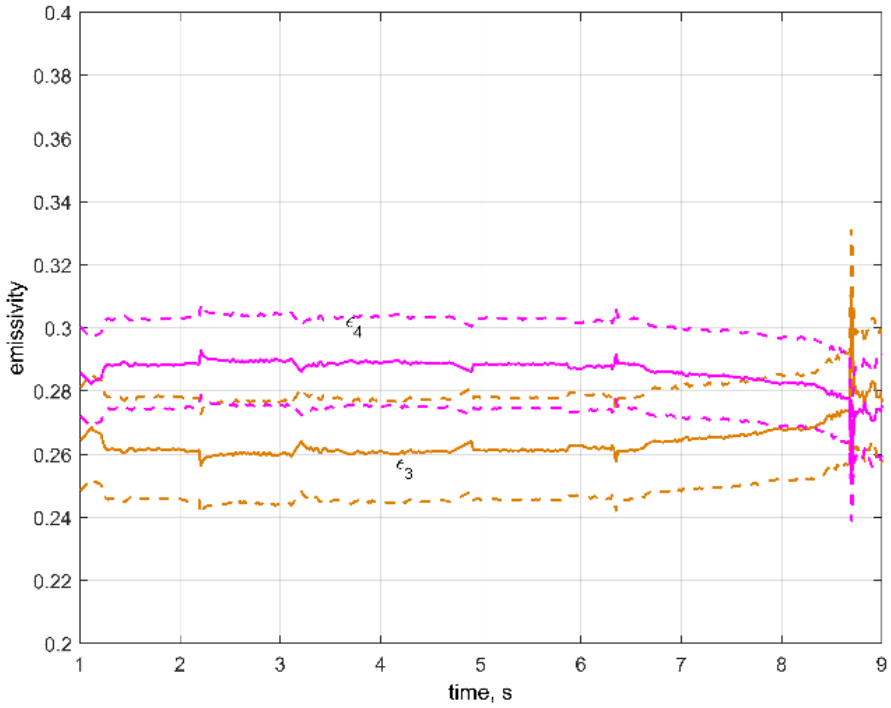

Figure 18. MAP estimator of emissivity ε_3 (in orange) and ε_4 (in violet) and plus or minus one standard-deviation (dashed lines).

Figures 15 and 16 show the normalized probability densities for the three parameters. On the solidification plateau, the mean and standard-deviation of the emissivities are $\varepsilon_3 = 0.261 \pm 0.023$ and $\varepsilon_4 = 0.288 \pm 0.020$ and for the temperature $T = (2\,748 \pm 29)$ K. The emissivities previously obtained with the OLS method are close, but 7 % higher: $\varepsilon_3 = 0.278 \pm 0.009$, $\varepsilon_4 = 0.300 \pm 0.008$. The method has then been extended to the whole duration of the experience by levering the previous results. As a matter of fact, since we have now a better confidence into the emissivity values, we considered as new priors $\varepsilon_3^{prior} = 0.260 \pm 0.023$ and $\varepsilon_4^{prior} = 0.290 \pm 0.020$, whereas temperature was given a prior of reduced quality since it is expected to evolve widely during the experiment: $T^{prior} = (2\,000 \pm 1\,000)$ K.

The results of this second identification phase are described in Figures 17 and 18. The MAP estimator of the emissivity ε_3 and ε_4 are quite stable in the liquid phase. On the contrary, in

the solid phase, ε_3 shows a slight increase whereas ε_4 shows a slight decrease. The mean standard-deviation of the estimator of temperature is between 7 and 32 K during the period [1s, 9s] of the experiment.

For the case of non-linear approximation, still with the measurements of OP#3 and OP#4, the estimation has been performed during the whole experiment and only two parameters are considered: the temperature and the emissivity ε_{34}. The Markov chains were started with parameters with the same priors as previously (of good quality for the temperature and bad quality for the emissivity). The chains were run with 30 000 states and the 15 000 first states were neglected for the computation of the posterior statistics (burn-in period). Figures 19 and 20 show the good fitting between the experimental and estimated flux and temperature, respectively. The 2.5 % and 97.5 % quantiles have also been calculated and presented in these figures, for the verification of the estimated fluxes and temperature versus the experimental ones.

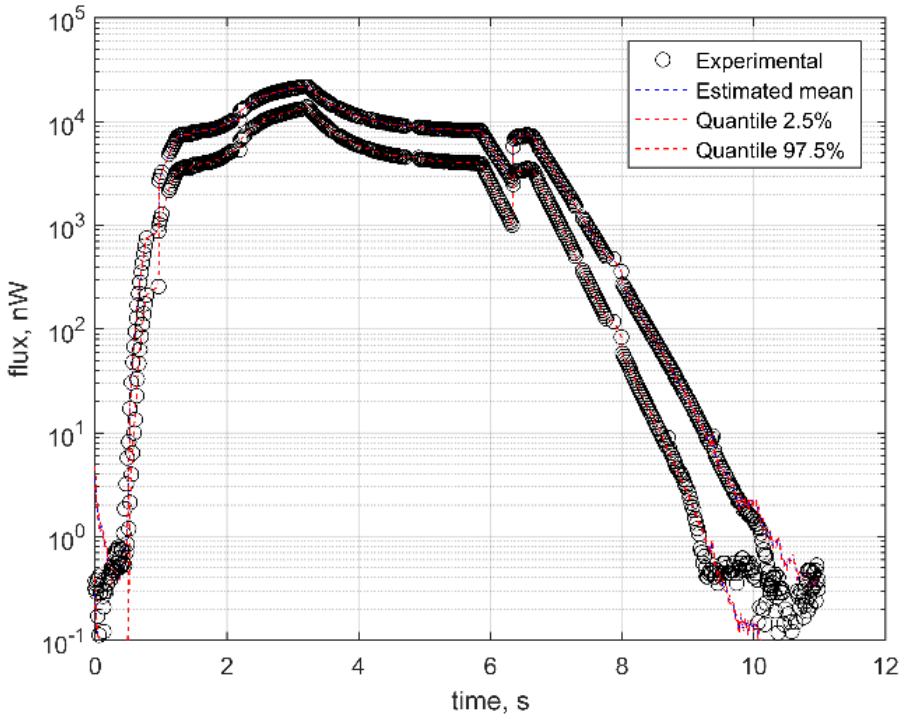

Figure 19. Estimated and experimental fluxes.

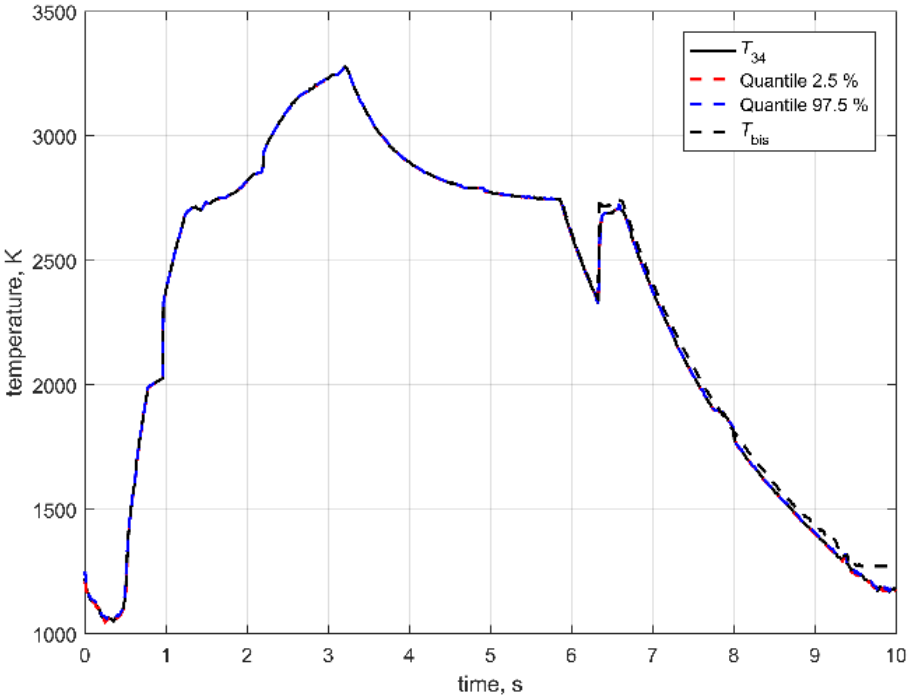

Figure 20. Estimated and experimental temperatures.

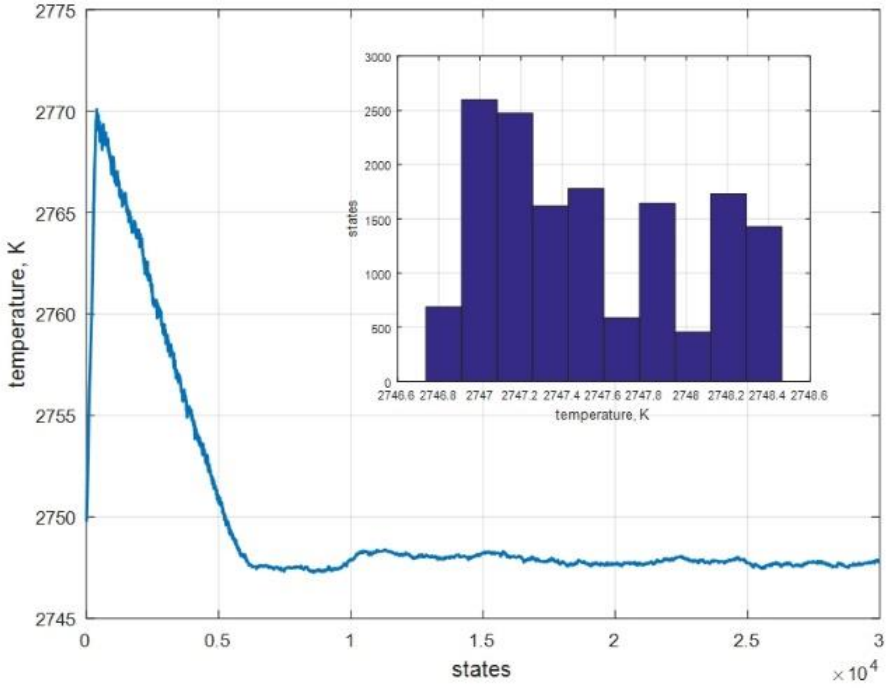

Figure 21. Markov chain states for the temperature estimation.

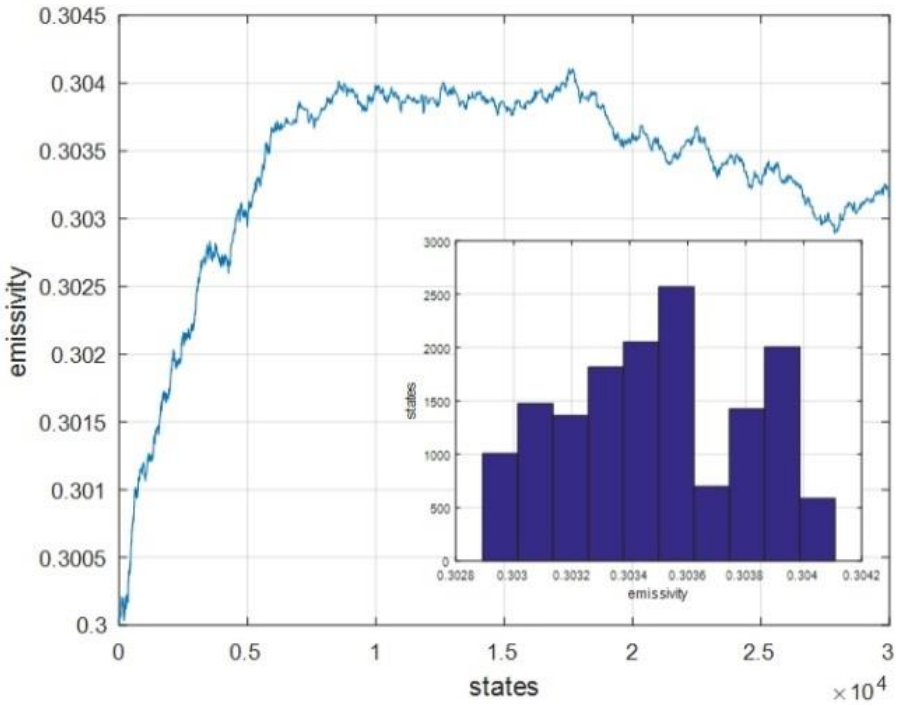

Figure 22. Markov chain states for the emissivity estimation.

Finally, Figures 21 and 22 presents the states of the Markov chains for both the temperature and emissivity at t = 6.7 s, that is, during the solidification plateau. They clearly show that the estimation tends to a rather constant value after 10 000 states. The histograms plotted for values after 15 000 states are not of Gaussian shapes, especially as regards the temperature. The prior for the temperature was centered at values at previous time with a constant standard deviation of 300 K, while the prior for the emissivity was considered as uniform in the interval [0, 1]. The estimated values for the solidification plateau are T = (2 747 ± 2) K, ε_{34} = 0.303 ± 0.002.

5.2. Estimation with steel sample

This last part concerns some results for the 100c6 steel, also referenced as AISI 52100 by ASTM [14]. Only Bayesian results are presented for this material with the linear

approximation and the non-linear case. Figure 23 presents the experimental fluxes measured with the multispectral pyrometer and the temperature T_{bis} with an emissivities ratio adjusted at 1.025. The fluxes measured by means of OP#1 and OP#2 are too weak to be used for the parameter estimation. As before, bispectral estimations are presented from the measurements of OP#3 and OP#4.

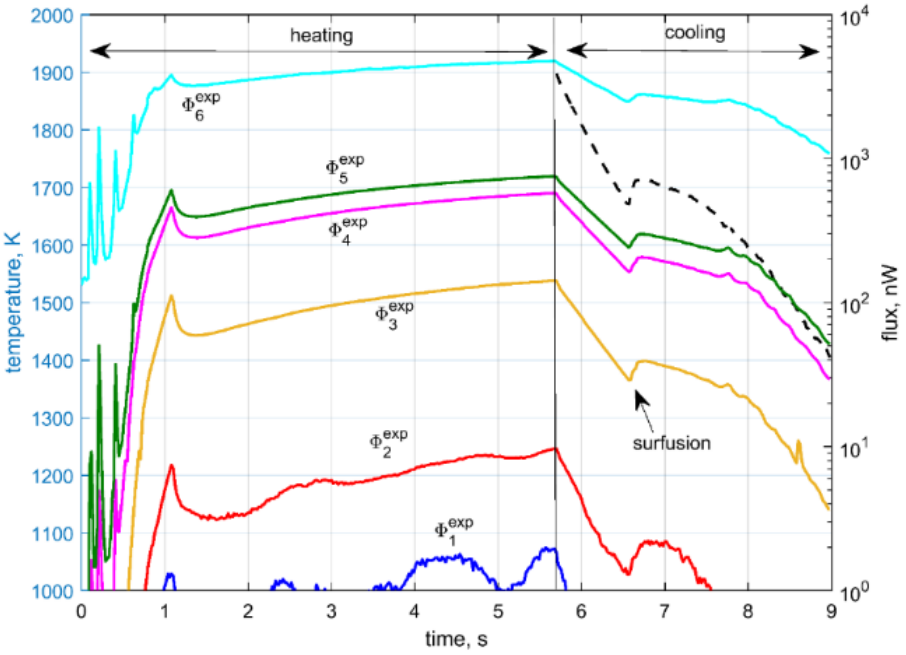

Figure 23. 100c6 steel sample fluxes.

The priors for the temperature and the emissivities are, respectively, T^{prior} = (1 700 ± 30) K and $\varepsilon_3^{prior} = \varepsilon_4^{prior} = 0.30 \pm 0.15$ according to literature data. We consider only the area of the solidification plateau, which does not appear clearly since the sample is an alloy.

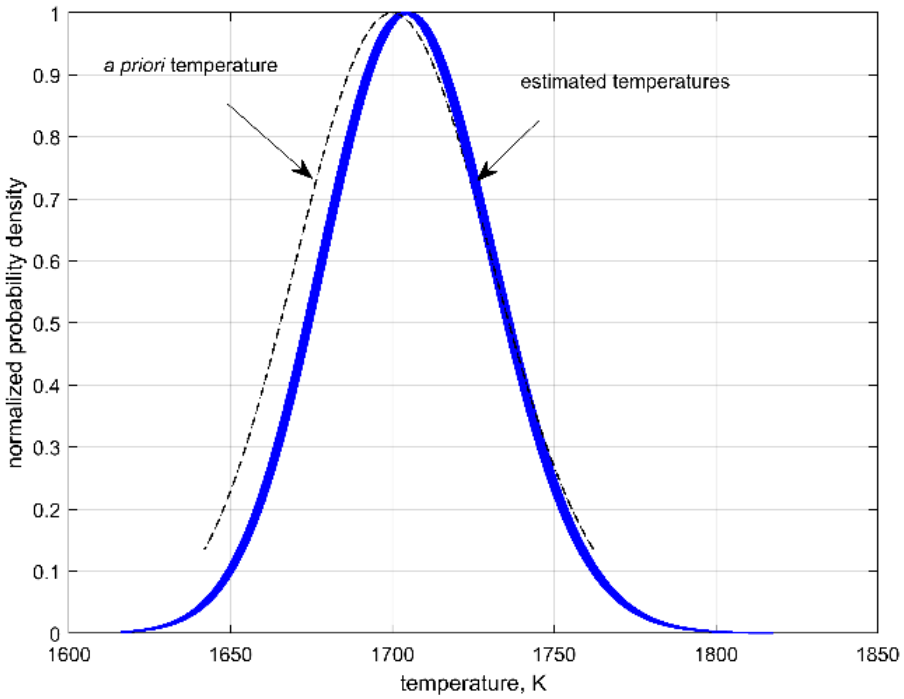

Figure 24. Estimated temperature through Bayesian inference with linear approximation.

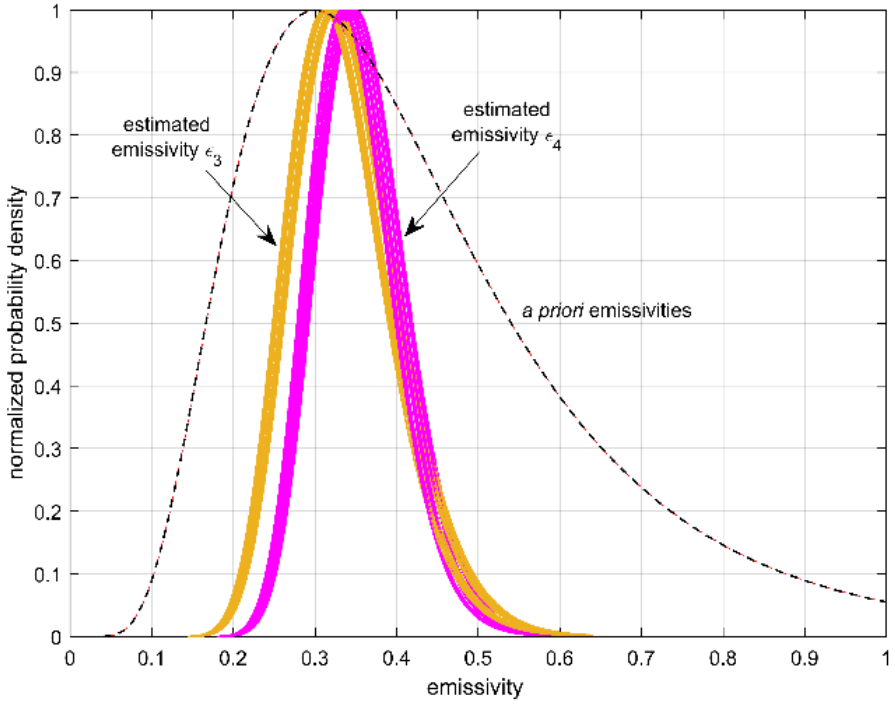

Figure 25. Estimated emissivities through Bayesian inference with linear approximation.

Figures 24 and 25 plot the normalized probability density of the estimated temperature and emissivities, whereas Figures 26 and 27 plot the estimated parameter-value evolution versus the Markov chain states (run with 100 000 states). First, the linear approximation and the non-linear methods give the following results: T = (1 703 ± 28) K, ε_3 = 0.328 ± 0.074, ε_4 = 0.351 ± 0.062, and T = (1 720 ± 7) K, ε_{34} = 0.296 ± 0.010, respectively. These values are averages of the range corresponding to the solidification plateau. The Markov chain shows rather constant values after the second half of the 100 000 states and a histogram with Gaussian shape. However, it is not plotted here, but we can note that the estimated temperatures fit rather well with the commercial bispectral pyrometer temperature T_{bis} along the whole cooling period (from 5.6 s to 9.0 s) giving credit to the priors.

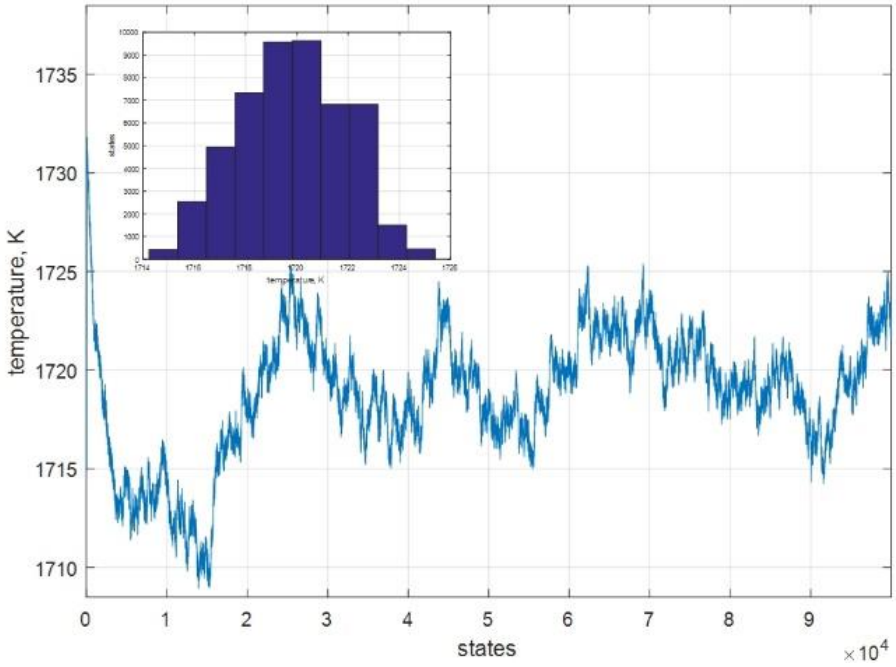

Figure 26. Estimated temperature versus Markov chain states with non-linear Bayesian.

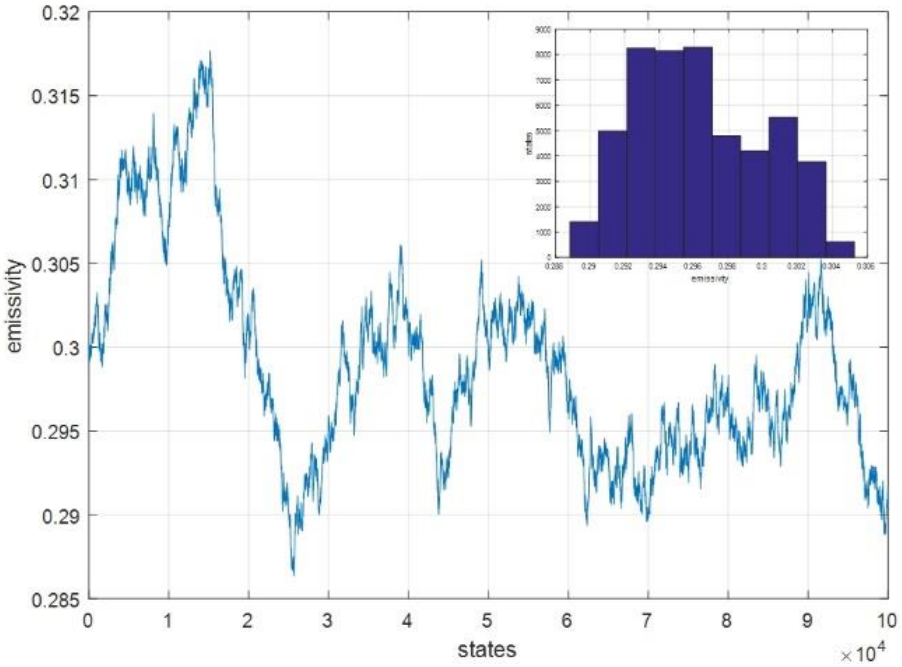

Figure 27. Estimated emissivity versus Markov chains states with non-linear Bayesian.

6. Conclusion

The article presented the first steps of the simultaneous temperature and emissivity estimation of molten metals by multispectral pyrometry using both deterministic and Bayesian techniques. Estimations were focused on bispectral pyrometry and one case by the multispectral method. The materials, niobium and steel samples, were aerodynamically levitated, then heated by laser above their melting point then cooled until room temperature. Radiative flux measurements have been performed with the help of a multispectral pyrometer, whereas a second commercial bispectral pyrometer measured the temperature as a supplementary information. The estimation results have shown that all techniques presented similar temperature and emissivity values consistent with the literature.

Nevertheless, whatever the considered multispectral pyrometry, both temperature and emissivity are not easy to estimate since, firstly, they are correlated parameters, and, secondly, the problem is ill-posed since the number of unknown is always one more than the number of information. In the case of the bispectral pyrometry and the multispectral pyrometry with m = 0 (constant emissivity), the current approach to assume a greybody hypothesis, considering

two measurements at two wavelengths, was not successful in this study. On the contrary, bispectral pyrometry with $\xi_{ji} \neq 1$ and multispectral pyrometry in the case of a linear emissivity ($m = 1$) gave better temperature values. Concerning the Bayesian technique, it has been necessary to take into account prior information, namely the emissivity, encountered in the literature and the temperature measured by the commercial bispectral pyrometer. However, it must be clear that the latter information was used only for initial calibration and for validation. Its systematic use is of course not needed. Nevertheless, with this information, the three tested methods give satisfying results, but need to be improved. The detection and the rigorous quantification of the uncertainties are of prime importance; it concerns for instance the calibration with a blackbody, which should be improved (*e.g.* blackbody ratio length/diameter [21]). Even if they are necessary in the Bayesian inference ($\pi(\boldsymbol{\beta})$), the major point to solve concerns the fact that we must use external information (priors) to commit estimation, due to the strong correlation between temperature and emissivity. Since the Bayesian techniques seem relevant to circumvent the ill-posed problem, it would be appropriate to couple this methodology with temperature-emissivity separation considerations [3][12]. It is all the more appropriate, since we have to consider emissivity variation due to phase changes, for instance oxidation.

References

[1] D Le Maux et al, *Density measurement of liquid 22MnB5 by aerodynamic levitation*, Review of Scientific Instrum., 90, 074904, 2019.

[2] B Lamien et al, *A Bayesian Approach for the Simultaneous Estimation of the Thermal Diffusivity and Thermal Conductivity of Aerodynamically Levitated Solid Metals at High Temperatures - Theoretical Study*, International Journal of Heat and Mass Transfer, 141, p. 265-281, 2019.

[3] J-C Krapez, *Radiative measurements of temperature* in *Thermal Measurements and*

Inverse Techniques (Taylor & Francis).

[4] T Pierre et al, *Micro-scale temperature by multi-spectral and statistic method in the UV-visible wavelengths*, J. Appl. Phys. 103(3), p. 1-10, 2008.

[5] T Duvaut et al., *Multiwavelength infrared pyrometry: optimization and computer simulations*, Infrared Physics & Technology 36 (1995) 1089-1103.

[6] P B Coates 1981 *Multiwavelength pyrometry* Metrologia 17 (1981) 103-109.

[7] J L Gardner, Computer modeling of a multiwavelength pyrometer for measuring true surface temperature, High Temperature – High pressures, 1980, volume 12, pages 699-705.

[8] C Rodiet et al., *Optimisation of wavelength selection used for the multi-spectral temperature measurement by ordinary least squares method of surfaces exhibiting non-uniform emissivity*, Quantitative Infrared Thermography, 2013.

[9] P Heasler, et al. *Nonlinear Bayesian Algorithms for Gas Plume Detection and Estimation from Hyper-Spectral Thermal Image Data* Sensors, vol. 7, n° 6, juin 2007, p. 905-20.

[10] C Berrett, et al. *A Bayesian Nonparametric Model for Temperature-Emissivity Separation of Long-Wave Hyperspectral Images* Technometrics, vol. 56, n° 2, avril 2014, p. 200-11.

[11] J N Ash, J Meola, *Temperature-emissivity separation for LWIR sensing using MCMC.* SPIE vol. 9840 (2016) 98401O.

[12] J-C Krapez, *Measurements without contact in heat transfer. Part A: radiative thermometry: principles, implementation and pitfalls*, Lecture 4 from METTI 7 advanced School, Volume 1: Lectures, Porquerolles, France, Sept. 29th – Oct. 4th, 2019.

[13] A Seifter et al. *Microsecond Laser Polarimetry for Emissivity Measurements on Liquid*

Metals at High Temperatures—Application to Niobium. International Journal of Thermophysics, vol. 22, n° 5, septembre 2001, p. 1537-47.

[14] http://www.astmsteel.com/product/52100-bearing-steel-aisi/ seen in january the 13th, 2020.

[15] R Siegel, J Howell, Thermal radiation heat transfer, Ed. Taylor & Francis), New-York, 2002.

[16] C Rodiet et al, *Optimal wavelengths obtained from laws analogous to the Wien_s law for monospectral and bispectral methods, and general methodology for multispectral temperature measurements taking into account global transfer function including non-uniform emissivity of surfaces*, Physics and Technology, 76, p. 444-454, 2016.

[17] C Rodiet et al, *Influence of measurement noise and number of wavelengths on the temperature measurement of opaque surface with variable emissivity by a multi-spectral method based on the flow ratio in the infrared-ultraviolet range*,High Temperatures-High Pressures, vol. 44, 2015.

[18] J Kaipio, E Somersalo, *Statistical and computational inverse problems*. Springer Science & Business Media 2006.

[19] Y S Touloukian, *Thermal radiative properties*, Plenum, New York, 1970.

[20] F P Incropera, D P DeWitt, *Fundamentals of Heat and Mass Transfer*, Wiley, 5th Edition, New-York, 2002.

[21] A Cezairliyan et al., *High-speed (subsecond) measurement of heat capacity, electrical resistivity, and thermal radiative properties of molybdenium in the range 1900 to 2800 K*, J. Res. Nat. Bur. Stand. 74A: 65-92 (Jan-Feb 1970), janvier 1970.